Supplemental Material: Boosting proximity spin orbit coupling in graphene/WSe_2 heterostructures via hydrostatic pressure

Bálint Fülöp,[1] Albin Márffy,[1] Simon Zihlmann,[2] Martin Gmitra,[3] Endre Tóvári,[1] Bálint Szentpéteri,[1] Máté Kedves,[1] Kenji Watanabe,[4] Takashi Taniguchi,[5] Jaroslav Fabian,[6] Christian Schönenberger,[2] Péter Makk (makk.peter@ttk.bme.hu),[1] and Szabolcs Csonka (csonka.szabolcs@ttk.bme.hu)[1]

[1] *Department of Physics, Budapest University of Technology and Economics and Nanoelectronics "Momentum" Research Group of the Hungarian Academy of Sciences, Budafoki út 8, 1111 Budapest, Hungary*
[2] *Department of Physics, University of Basel, Klingelbergstrasse 82, CH-4056 Basel, Switzerland*
[3] *Institute of Physics, Pavol Jozef Šafárik University in Košice, Park Angelinum 9, 040 01 Košice, Slovak Republic*
[4] *Research Center for Functional Materials, National Institute for Materials Science, 1-1 Namiki, Tsukuba 305-0044, Japan*
[5] *International Center for Materials Nanoarchitectonics, National Institute for Materials Science, 1-1 Namiki, Tsukuba 305-0044, Japan*
[6] *Institute for Theoretical Physics, University of Regensburg, 93040 Regensburg, Germany*

(Dated: July 7, 2021)

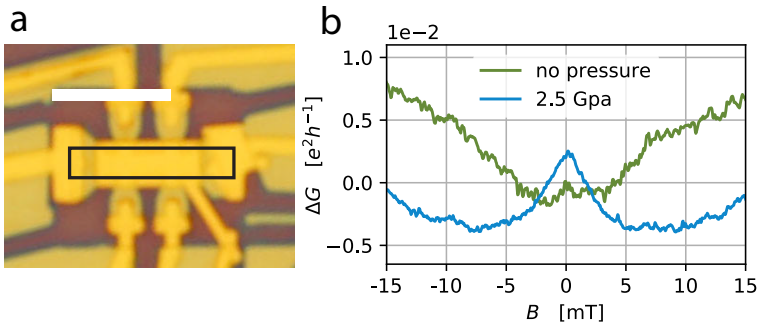

Supplementary Figure 1. Measurements of device B. (a) Optical micrograph of the device with the studied segment highlighted by black rectangle. This heterostructure consists of the same layers as device A, and the measured two-terminal segment was $L = 5\,\mu m$ long and $W = 1\,\mu m$ wide. 4 terminal voltage was measured on the electrodes of the lower side of the picture, but not used during the analysis discussed here. The electrodes on the upper side were left floating. (b) Two terminal magneto-conductance signal, averaged between $+2\,V$ and $+4\,V$ from the charge neutrality point. This device also exhibits an increasing WAL peak at higher pressures, but a proper comparison of the pressures was not possible due to gate instabilities and drifts.

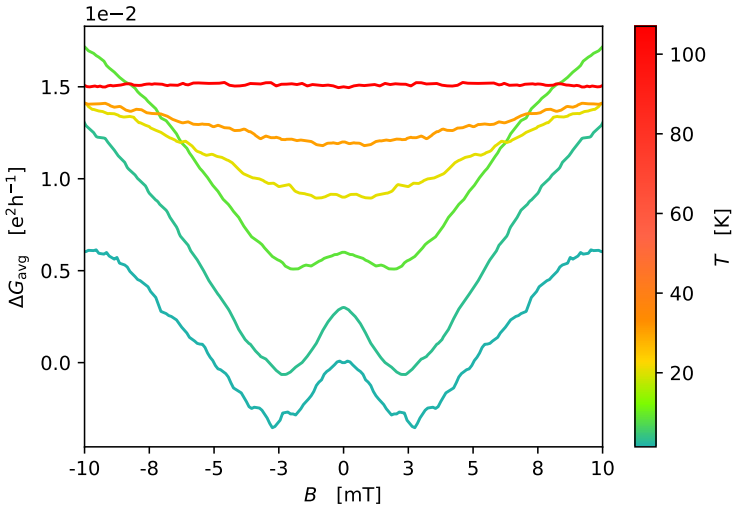

Supplementary Figure 2. Temperature dependence of the symmetrized magneto-conductance curves at maximum pressure ($p = 1.8\,\mathrm{GPa}$) with averaging between 0 V and 2 V gate voltage. The amplitude of the WAL peak decreases with increasing temperature due to the reduction of τ_φ and the background is negligible above 30 K at low magnetic fields. The curves are shifted by $0.003\,e^2/h$ for clarity.

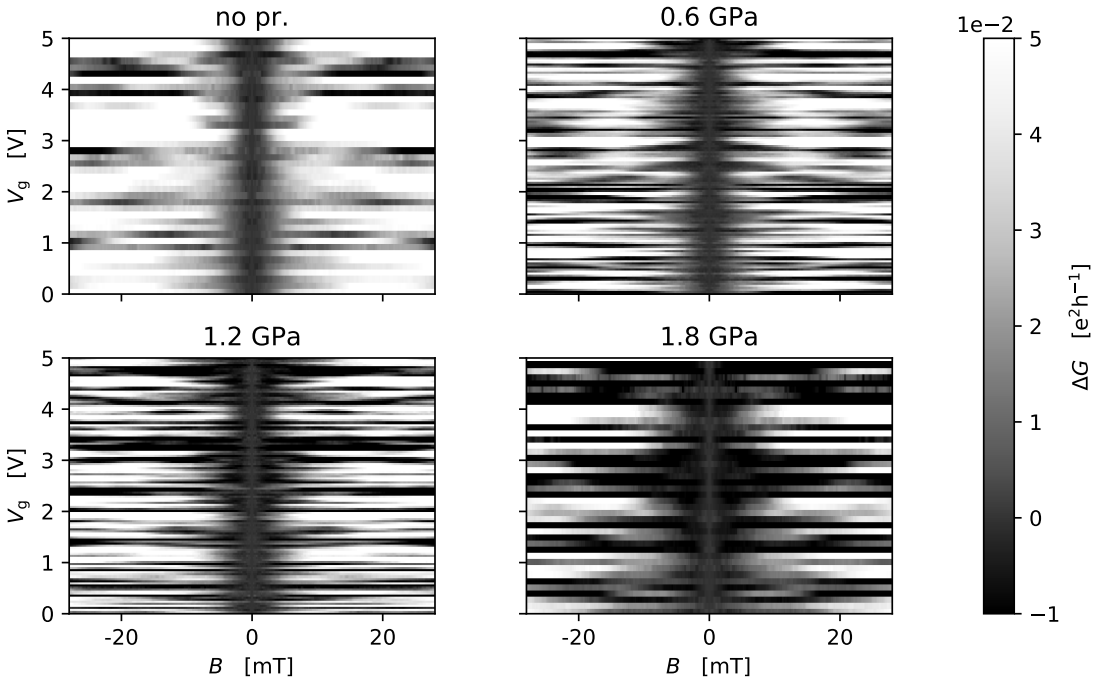

Supplementary Figure 3. Symmetrized magneto-conductance correction vs. gate voltage V_g and magnetic field B for all measurements. The colorbar and the axes values are the same for each map. A vertical gray line $\Delta G = 0$ at $B = 0$ is visible on all maps due to the correction method. A darker gray shoulder becomes more and more visible along the V_g axis as pressure rises at low magnetic fields ($B < 5\,\mathrm{mT}$). At higher magnetic fields ($B > 5\,\mathrm{mT}$) universal conductance fluctuations (UCF) become dominant leading to irregular magneto-conductance curves. The colorbar is set to resolve the peak appearance in the low magnetic regime, thus the signal of UCF saturates it.

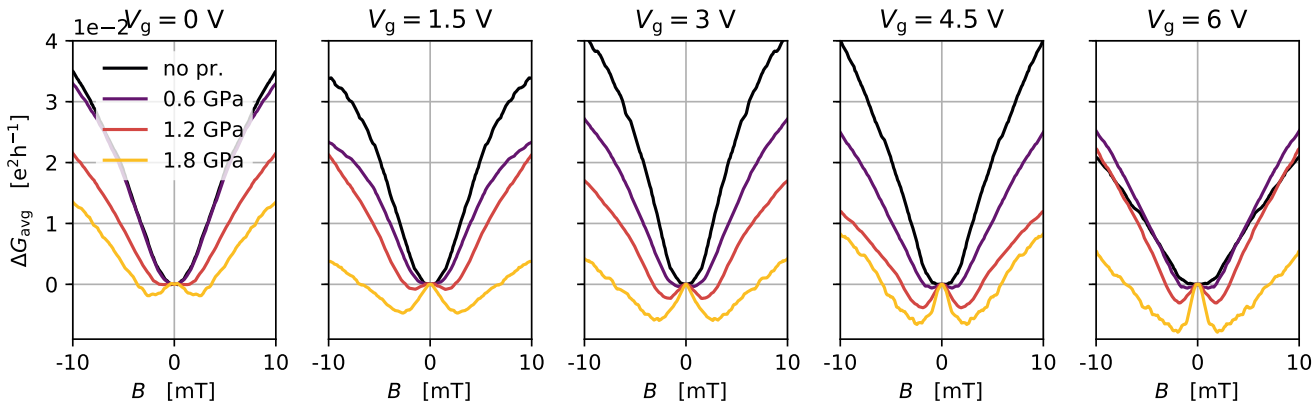

Supplementary Figure 4. Detailed comparison of symmetrised and averaged magneto-conductance curves at different gate voltages. Each curve is made by an averaging of all the recorded curves within a ± 1.5 V range around the value indicated in the panel title. The colors mark the same pressure on each plot. The WAL peak is more pronounced at all gate voltages as the pressure is increased, which suggests that the increasing pressure has an influence on the enhanced WAL feature independently on other, gate-dependent scattering mechanisms. Conductance correction above 5 mT includes a pronounced contribution of UCF which leads to irregular curve shapes. In addition, gate voltage dependence of the line shape is also clearly visible. The peak amplitude grows with the gate voltage, which is in agreement with Ref. [1] and can be explained with the change of other time scales along with the ones associated to SOC. This tendency is present at every pressure. Due to this dependence on gate voltage, one has to find a balance between reducing the effect of UCF sufficiently and not to average over a gate voltage range where the physical processes differ too much. After investigating the gate voltage measurements and magneto-conductance curves averaged over different gate voltage ranges, we found that the curves of $4\,\text{V} \pm 1.5\,\text{V}$ give a good compromise. This is the setting we used for the fitting.

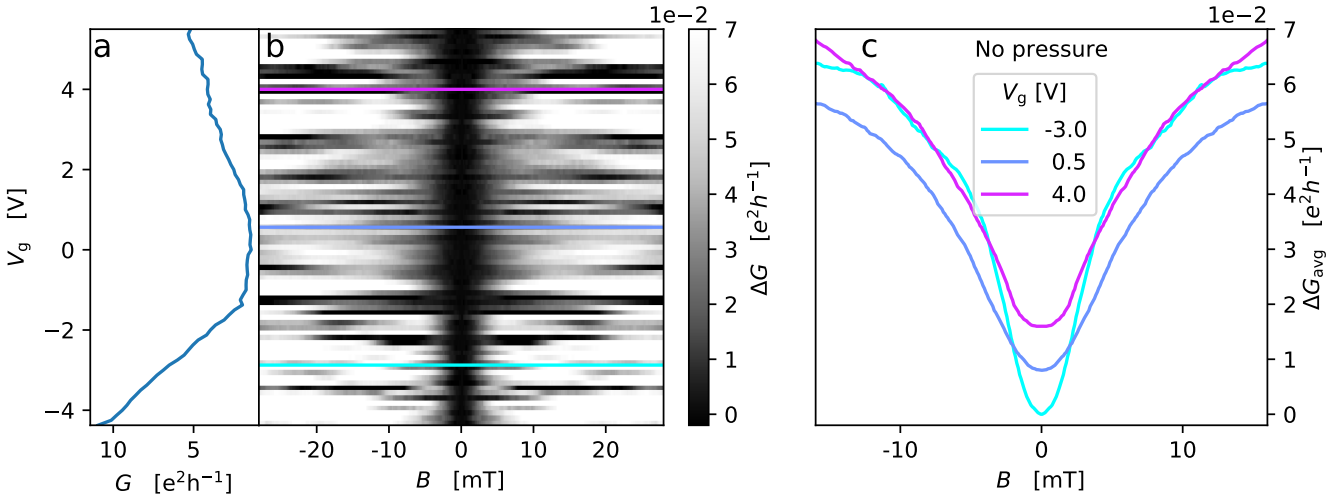

Supplementary Figure 5. Weak localization measurement at ambient pressure at the end of the experiment, after releasing the hydrostatic pressure. (a) Two-terminal zero-field conductance $G(V_g, B = 0)$. (b) 2D grayscale plot of the symmetrized two-terminal conductance corrected by the zero-field conductance $\Delta G(V_g, B) = G(V_g, B) - G(V_g, B = 0)$. (c) Magneto-conductance curves at fixed gate voltages marked in panel b with ± 1.5 V averaging along the vertical axis to reduce the effect of UCF. The curves are shifted by $0.01\, e^2/\mathrm{h}$ for clarity. The observed features are similar to that of the initial ambient pressure measurement: at small magnetic fields ($B < 5$ mT) a WL dip is recovered at all gate voltages.

SUPPLEMENTARY NOTE 1

If the scattering times of the SOC ($\tau_{\rm asy}, \tau_{\rm sym}$) are comparable to the intervalley scattering time ($\tau_{\rm iv}$), both SOC and chirality influences the magneto-conductivity at the same B field scale, and a unified formula is needed to describe the weak localization behaviour. This can be derived from Ref. [2], as has been done in Ref. [3]:

$$\begin{aligned}\Delta\sigma(B) = -\frac{1}{2}\frac{e^2}{\pi h}\Bigg[&F\left(\frac{\tau_B^{-1}}{\tau_\varphi^{-1}}\right) - F\left(\frac{\tau_B^{-1}}{\tau_\varphi^{-1}+2\tau_{\rm asy}^{-1}}\right) - 2F\left(\frac{\tau_B^{-1}}{\tau_\varphi^{-1}+\tau_{\rm asy}^{-1}+\tau_{\rm sym}^{-1}}\right)\\ &- F\left(\frac{\tau_B^{-1}}{\tau_\varphi^{-1}+2\tau_{\rm iv}^{-1}}\right) - 2F\left(\frac{\tau_B^{-1}}{\tau_\varphi^{-1}+\tau_{\rm iv}^{-1}+\tau_{\rm ia}^{-1}}\right)\\ &+ F\left(\frac{\tau_B^{-1}}{\tau_\varphi^{-1}+2\tau_{\rm iv}^{-1}+2\tau_{\rm asy}^{-1}}\right) + 2F\left(\frac{\tau_B^{-1}}{\tau_\varphi^{-1}+\tau_{\rm iv}^{-1}+\tau_{\rm ia}^{-1}+2\tau_{\rm asy}^{-1}}\right)\\ &+ 2F\left(\frac{\tau_B^{-1}}{\tau_\varphi^{-1}+2\tau_{\rm iv}^{-1}+\tau_{\rm asy}^{-1}+\tau_{\rm sym}^{-1}}\right) + 4F\left(\frac{\tau_B^{-1}}{\tau_\varphi^{-1}+\tau_{\rm iv}^{-1}+\tau_{\rm ia}^{-1}+\tau_{\rm asy}^{-1}+\tau_{\rm sym}^{-1}}\right)\Bigg],\end{aligned} \tag{1}$$

where $\tau_{\rm ia}^{-1}$ is a scattering rate due to the intravalley scattering due to soft potentials and to the trigonal warping, together. This 5-parameter formula simplifies to the 3-parameter formula used in the main text if $\tau_{\rm iv}^{-1}, \tau_{\rm ia}^{-1} \ll \tau_\varphi^{-1}, \tau_{\rm asy}^{-1}, \tau_{\rm sym}^{-1}$. Remarkably, this complete formula is invariant under the pairwise interchange of rates ($\tau_{\rm asy}^{-1}, \tau_{\rm sym}^{-1}$) and ($\tau_{\rm iv}^{-1}, \tau_{\rm ia}^{-1}$), i.e. chirality and SOC contribute to the magneto-conductivity in the same manner. We note that we present this form of the expression instead of using the commonly used substitution of $\tau_*^{-1} = \tau_{\rm iv}^{-1} + \tau_{\rm ia}^{-1}$ to emphasize the symmetry of SOC and scattering parameters. This symmetry makes the interpretation of the fit variables ambiguous unless the value of at least one of the parameters can be determined via an independent measurement. We assume that the momentum relaxation time $\tau_{\rm m}$, extracted from the gate voltage measurements for each pressure, corresponds to the intravalley scattering time $\tau_{\rm ia}$, which is shorter than any other time scale. Therefore, during curve fitting, the measured value of $\tau_{\rm m}$ is used as the value of the fixed parameter $\tau_{\rm ia}$ leaving only 4 parameters to optimize; and as a lower bound for all other time parameters for both the 3-parameter and the 5-parameter formulas.

Due to the complex shape of the fit formulas, one can expect multiple fit parameter sets that approximate a measured signal reasonably well. To assess the uncertainty associated to the fitting parameters of this origin, we introduce a fitting method called "grid fit" that is described in the following. During the curve fitting of a single magneto-conductivity curve, we do not search for the global best fit, but we look for all the sufficiently good fits in the parameter space. To this end, we create a grid of starting parameters in the 3D parameter space of ($\tau_\varphi, \tau_{\rm asy}, \tau_{\rm sym}$) for the 3-parameter formula, or the 4D parameter space ($\tau_\varphi, \tau_{\rm asy}, \tau_{\rm sym}, \tau_{\rm iv}$) of the 5-parameter formula (as $\tau_{\rm ia}$ is fixed), and we start a Levenberg-Marquardt fitting algorithm at each grid point. We accepted the fit if the reduced chi-squared statistic of the fit result was reasonably close to the best value observed in the whole grid. The start points' grid extends for each time parameter from the actual value of $\tau_{\rm m}$ for each pressure to an upper limit of $1 \cdot 10^{-11}$ s, which we consider as a reasonable upper limit for τ_φ at the measurement temperature and therefore for any other time scale that has a visible influence on the magneto-conductivity curves. Since we looked at parameter values extending over multiple order of magnitude, the distribution of the grid points for each parameter was log-uniform, i.e. the values of $\ln \tau_{\rm i}$ were equidistant for $i \in \{\varphi, {\rm asy}, {\rm sym}\}$ in the studied range.

All the accepted fits approximate the measurement data equally well for both formulas, with point-to-point differences of the curves 3 orders of magnitude smaller than the measurement values. In Figure 6b-c, a summary of the fit parameters is shown as an example for the grid fit of the 0.6 GPa curve using the 5-parameter formula. The result of each executed fit is represented by a pair of points on the two panels. The position of the points correspond to the fit values of the parameters marked on the axes, and the red color marks the accepted fits. Fits that were a result of the Levenberg-Marquardt algorithm started from a parameter grid point but got rejected due to their high reduced chi-squared statistic are marked by blue. For the parameters $\tau_\varphi, \tau_{\rm asy}, \tau_{\rm iv}$ the accepted fit values are concentrated on a small part of the studied range which suggests reliable fit values. However, similarly to the results using the 3-parameter formula, the value of $\tau_{\rm sym}$ can vary across orders of magnitude without decreasing the fit goodness, meaning that the valley–Zeeman effect does not have any measurable effect on the weak localization behavior in this experiment. Therefore we conclude that the method can not extract reliable value for $\tau_{\rm sym}$.

For the other parameters, we consider all the accepted outcomes as physically valid values, since these parameter sets are equivalent in the curve shape. We attribute the geometric mean of the maximum and the minimum of the accepted values as the fit value of the parameter and the upper and lower error boundaries are the minimum and maximum of the accepted outcomes. The results are summarized in Figure 6d. The fit values of τ_φ and $\tau_{\rm asy}$ are very

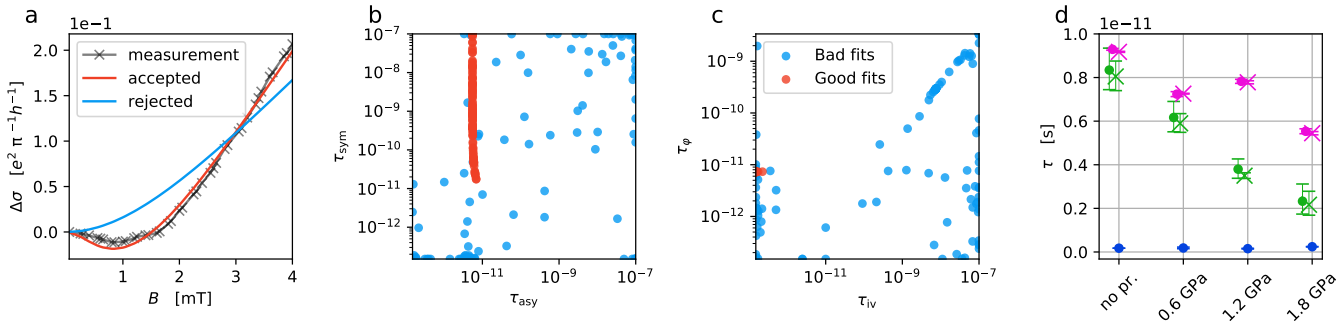

Supplementary Figure 6. (a) Example of accepted (red) and rejected (blue) fit results using the 3-parameter formula on the 0.6 GPa curve. Fit results were accepted based on their reduced chi-squared statistic. (b-c) Summary plots of the fit parameters of the accepted fits to the 0.6 GPa measurement data curve using the complete formula, shown as an example. Every result of the Levenberg-Marquardt method is represented by a pair of dots at the fit value of all the 4 fit parameters. Red dots represent fits that approximate the measurement data reasonably well. Blue dots represent the rejected fit results. (d) Comparison of fit parameters using the formulas. The pink color corresponds to τ_φ, the green one to τ_{asy}. The cross marker is the fit value using the 3-parameter formula, the dot using the 5-parameter formula. The errorbars represent the minimum and maximum values, the data point is the geometric mean value of the accepted fits. Using the 5-parameter formula, both τ_φ and τ_{asy} obtain values very close to the results of the 3 parameters formula. The values for τ_{iv} using the 5-parameter formula are also plotted with blue. Its small values compared to τ_φ and τ_{asy} validates the applicability of the 3-parameter formula. The data points are slightly shifted horizontally to avoid overlapping errorbars.

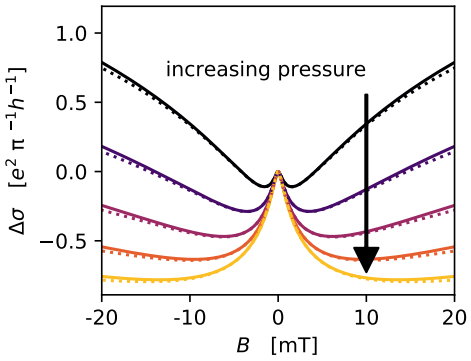

Supplementary Figure 7. Simulated weak anti-localization curves using both the 3-parameter (solid line) and 5-parameter (dotted line) formulas. The curves presented in the main text correspond to the solid lines. The difference of the two curve set is only visible at high magnetic fields, the shape of the central peak is unaffected. Therefore, the two formulas assess the spin orbit times similarly, which supports the parameter fit values in 6d.

close for both formulas and show the decreasing trend discussed in the main text. The values of τ_{iv} are indeed much smaller than the other time scales, which suggests that the influence of chirality is indeed negligible in our case and the 3-parameter formula is applicable. This is also demonstrated in Figure 7, where 5 pair of simulated curves of the same parameters are plotted using the 3-parameter and the 5-parameter formula. The 3-parameter curves are also shown in Figure 1b of the main text. The τ_{asy} and τ_{sym} parameters were calculated from the λ_{R} and λ_{VZ} parameters, respectively. For the simulation of the pressure, λ_{R} was changed from 300 µeV to 900 µeV in 5 equidistant steps, whereas λ_{VZ} was changed from 800 µeV to 2.0 meV in the same manner. The other parameters were fixed for all curves both for the calculation of the magneto-conductivity curves and of the SOC time parameters: $\tau_\varphi = 1 \cdot 10^{-11}$ s, $\tau_{\mathrm{iv}} = 1 \cdot 10^{-13}$ s, and $\tau_{\mathrm{ia}} = 1 \cdot 10^{-13}$ s. The difference between the 3-parameter and the 5-parameter curves is only visible at higher magnetic fields.

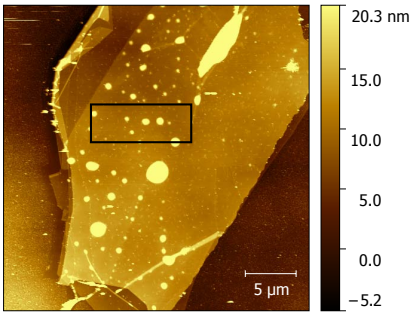

Supplementary Figure 8. AFM height map of the graphene surface prior to deposition of the top hBN flake for the the sample presented in the main text. The segment measured is roughly highlighted by the black rectangle. These measurements exhibit a considerable amount of contamination and bubbles between the component layers. This could weaken the interlayer coupling and reduce somewhat the SOC in our device.

[1] Tikhonenko, F. V., Horsell, D. W., Gorbachev, R. V. & Savchenko, A. K. Weak localization in graphene flakes. *Phys. Rev. Lett.* **100**, 056802 (2008). URL https://link.aps.org/doi/10.1103/PhysRevLett.100.056802.

[2] McCann, E. & Fal'ko, V. I. $z \to -z$ symmetry of spin-orbit coupling and weak localization in graphene. *Phys. Rev. Lett.* **108**, 166606 (2012). URL https://link.aps.org/doi/10.1103/PhysRevLett.108.166606.

[3] Zihlmann, S. *et al.* Large spin relaxation anisotropy and valley-zeeman spin-orbit coupling in wse_2/graphene/h-bn heterostructures. *Phys. Rev. B* **97**, 075434 (2018). URL https://link.aps.org/doi/10.1103/PhysRevB.97.075434.